SPACE-TIME-DOMAIN GAUSSIAN BEAM MIGRATION IN VTI MEDIA BASED ON THE UPWARD RAY TRACING AND ITS APPLICATION IN LAND FIELD DATA

DONGLIN ZHANG[1,2], JIANPING HUANG[1,2], JIDONG YANG[1,2], BIN ZHOU[3], JIANFENG ZHANG[3] and QINGYANG LI[4]

[1] *School of Geosciences, China University of Petroleum (East China), Qingdao 266580, P.R. China. dlzhang_upc@163.com; jphuang@upc.edu.cn*
[2] *Laboratory for Marine Mineral Resources, Pilot National Laboratory for Marine Science and Technology (Qingdao), Qingdao 266071, P.R. China.*
[3] *Geophysical China Oilfield Services Limited, Tianjing 300459, P.R. China.*
[4] *Geophysical Exploration Research Institute of Zhongyuan Oilfield Company, Puyang, 457001, P.R. China.*

(Received March 22, 2022; revised version accepted September 10, 2022)

ABSTRACT

Zhang, D.L., Huang, J.P., Yang, J.D., Zhou, B., Zhang, J.F. and Li, Q.Y., 2022. Space-time-domain Gaussian beam migration in VTI media based on the upward ray tracing and its application in land field data. *Journal of Seismic Exploration*, 31: 545-562.

Gaussian beam migration (GBM) method is an efficient and adaptable imaging tool, but the traditional GBM method may produce some false imaging in some layers due to the inaccurate ray tracing in the construction of reverse wavefields. Firstly, the reverse wavefields are constructed by using the upward ray tracing strategy. Then, we derive the space-time-domain GBM formula in acoustic medium based on the cross-correlation imaging condition. Finally, taking in account the anisotropic characteristics, we use the anisotropic ray tracing theory to implement a space-time-domain GBM approach in VTI media. After testing for the anisotropic graben and diffractor models as well as a land field data, compared with the imaging results in space-time-domain isotropic GBM, we get the following conclusions: 1) The diffraction energy of the graben model is more convergent in the low layers; 2) Our method can clearly image the diffracting points of the diffractor model; 3) For the field data, the image resolution is obviously improved, the fault planes are clearer, and the image amplitude in the left part of the anticline is more balanced.

KEY WORDS: Gaussian beam migration, upward ray tracing, space-time-domain, VTI, anisotropic.

0963-0651/22/$5.00

INTRODUCTION

With the development of oil and gas exploration, the underground medium has gradually become more complex. How to improve the imaging accuracy of the traditional migration methods has become a hot research topic for many scholars. The Gaussian beam migration (GBM) method is popular in seismic data processing because it can produce good imaging results as the wave-equation-based method and have high computational efficiency as the ray-based method. Its imaging framework mainly includes the traditional frequency domain and the recent space-time domain. The former has the characteristic of high efficiency, but due to inaccurate paraxial ray tracing, it might lead to some false offset in some structure; the latter uses inverse time extrapolation to construct the reverse wavefields and further improves the imaging accuracy at the cost of efficiency.

For the study of GBM, Hill (1990, 2001) first proposed the basic framework of GBM. He respectively proposed zero-offset and pre-stack depth GBM and gave the calculation formula of the relevant parameters. Gray and Bleistein (2009) proposed an amplitude-preserved imaging method based on Gaussian beam, which is beneficial to the seismic interpretation. Nowack (2011) proposed a focused beam migration method using a focusing idea. Based on the focused beam, Yang et al. (2015) developed an adaptive GBM approach by focusing and adjusting the beam shape with the velocity. Yuan et al. (2017) proposed a least-squares GBM, which produces better imaging results with less artifacts. Yang and Zhu (2018) proposed a GBM method using a real data-driven optimization strategy. In addition, many scholars developed GBM method to complex surface conditions (Yue et al., 2010, 2012; Huang et al., 2016; Han et al. 2020), elastic media (Protasov and Tcheverda, 2012; Huang et al., 2017) and viscous media (Bai et al., 2016; Yue et al., 2021).

Based on the anisotropy theory, Červený (1972) first proposed the ray tracing theory in Vertical Transversely Isotropic (VTI) medium and gave a detailed derivation of the relevant formula. Hanyga (1986) derived a GBM imaging method based on elastic anisotropic media, which was further applicable to the actual situation of complex earth media. To solve the anisotropic ray tracing equation, Alkhalifah (1995) simplified the anisotropic ray tracing equation and derived a frequency-domain GBM method applicable to VTI media. Zhu et al. (2007) proposed a pre-stack migration approach of Gaussian beam in anisotropic media, which can produce better images than anisotropic pre-stack Kirchhoff migration. Han et al. (2014) developed GBM to Transversely Isotropic (TI) media based on converted waves. Han et al. (2017) used anisotropic kinematic and dynamic ray tracing systems to get an angle-domain GBM method. Li et al. (2018) derived the ray tracing equation of converted wave in VTI media using the ray tracing algorithm of anisotropic media, developed a ray tracing algorithm of converted wave, and proposed a GBM method of converted wave in the angle domain in VTI media. Han et al. (2021) proposed a nonslant stack beam migration for multicomponent seismic data in VTI media.

GBM in space-time domain is used to construct the forward and reverse wavefields using the Gaussian beam stack, and finally realize the migration imaging process. It mainly includes Gaussian packet migration (Žáček, 2006) and Gaussian beam inverse time migration (Popov et al., 2010). Li et al. (2014) used Gaussian packet propagator to characterize seismic wavefields in Gabor transform domain and realized a feature Gaussian pre-packet migration method. Hu et al. (2020) separated pure P wave and S wave of vector wavefields by elastic reverse-time migration method and realized a multi-wave space-time-domain GBM method for elastic media by modifying inner product imaging conditions.

In order to ensure that the proposed method has high imaging accuracy and is suitable for complex anisotropic media, we first construct the time-reverse wavefields based on the upward ray tracing strategy. Then we calculate the travel time and amplitude information of Gaussian beam in VTI media accurately using anisotropic ray tracing theory and develop a space-time-domain VTI GBM method based on cross-correlation imaging conditions. In the end, we use two anisotropic models to test its correctness and have some application to the field data.

THEORY

Space-time-domain Gaussian beam

As in Fig. 1, in 2D ray central coordinates, the seismic wavefields excited by the point source function $g(t)$ in acoustic medium can be expressed as

$$\Delta U(\mathbf{r},t)-\frac{1}{v^2}\frac{\partial^2 U(\mathbf{r},t)}{\partial t^2}=g(t) \quad , \tag{1}$$

where $U(\mathbf{r},t)$ are the seismic wavefields, $\mathbf{r}=(s,n)$ is the spatial coordinate position of the seismic wave in 2D ray central coordinate system, v and t are the speed and time of seismic wave propagation, respectively.

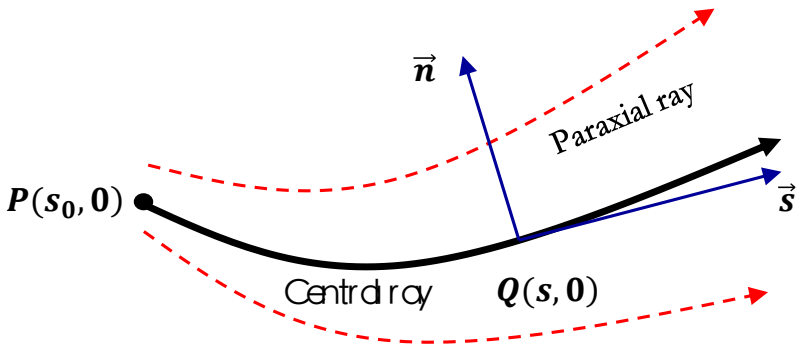

Fig. 1. The 2D ray centered coordinates in the vicinity of a ray.

According to Kachalov and Popov (1988), the Gaussian beam could be expressed the following form

$$U_{\mathrm{GB}} = -\frac{\mathrm{i}}{4\pi}\int \mathrm{d}\omega \sqrt{\frac{\varepsilon(s_0)v(s)}{v(s_0)Q(s)}} \exp\left[\mathrm{i}\omega\left(-(t-\tau)+\frac{1}{2}\frac{P(s)}{Q(s)}n^2\right)\right], \tag{2}$$

where $\mathbf{x_0}$ and $\mathbf{x}_s$ are the spatial coordinate position of the image and shot points, respectively. ε is the initial Gaussian beam parameter, ω is the circular frequency of the seismic data, τ is the travel time, s_0 is the initial spatial coordinate position in 2D ray central coordinate system, s and n are tangential and vertical coordinates, respectively. $P(s)$ and $Q(s)$ can be expressed as the following form (Hill, 1990)

$$\begin{cases} \dfrac{\mathrm{d}Q(s)}{\mathrm{d}s} = v_0 P(s) \\ \dfrac{\mathrm{d}P(s)}{\mathrm{d}s} = -\dfrac{1}{v_0^{\,2}}\dfrac{\partial^2 v}{\partial n^2} Q(s) \end{cases}, \tag{3}$$

where v_0 is the initial velocity.

Anisotropic ray tracing

In isotropic media, the central coordinate systems of rays are orthogonal to each other, but when the anisotropic media is considered, the direction of rays is no longer perpendicular to the front of the wave. At this point, if the isotropic ray tracing theory is continued, it will lead to inaccurate calculation of travel time and amplitude information, and ultimately reduce the accuracy of the migration imaging results. Therefore, we introduce a weight along the ray direction to deal with this non-orthogonality, which can calculate more accurate parameters. It can accurately construct the central ray adjacent wavefields in VTI medium and provide favorable conditions for subsequent migration imaging results. Hanyga (1986) gave the dynamic ray-tracing equation in VTI media

$$\begin{cases} \dfrac{\mathrm{d}Q(s)}{\mathrm{d}\tau} = WQ(s) + VP(s) \\ \dfrac{\mathrm{d}P(s)}{\mathrm{d}\tau} = -HQ(s) - VP(s) \end{cases}, \tag{4}$$

where *W, V, H*, are the following form

$$\begin{cases} W = \dfrac{1}{2}\dfrac{\partial^2 R}{\partial {p_n}^2} - \dfrac{1}{4}\left(\dfrac{\partial R}{\partial p_n}\right)^2 \\ V = \dfrac{1}{2}\dfrac{\partial^2 R}{\partial p_n \partial n} - \dfrac{1}{4}\dfrac{\partial R}{\partial p_n}\dfrac{\partial R}{\partial n} \\ H = \dfrac{1}{2}\dfrac{\partial^2 R}{\partial n^2} - \dfrac{1}{4}\left(\dfrac{\partial R}{\partial n}\right)^2 \end{cases}, \tag{5}$$

where p_n is the component of slowness along *n*, which is perpendicular to the front of the wave. *R* is the eikonal function of the P wave, which can be written in the following form

$$R=\left(a_{11}p_1p_1 + a_{55}p_3p_3\right)g_1g_1 + 2\left(a_{11}+a_{55}\right)p_1p_3g_1g_3 + \left(a_{55}p_1p_1 + a_{33}p_3p_3\right)g_3g_3 \tag{6}$$

where $a_{ijkl} = \dfrac{c_{ijkl}}{\rho}$ is the result of density normalization for elastic parameter c_{ijkl}, g_j is the component of polarization vector and $p_i = \dfrac{\partial \tau}{\partial x_i}$ is the component of slowness with each direction in the rectangular coordinate system.

Construction of wavefields based on the upward ray tracing strategy

The forward wavefields can be formed by superposition of Gaussian beams emanating from different angles (Červený et al., 1982; Popov, 1982)

$$W^{(1)} = -\frac{\mathrm{i}}{4\pi}\int_0^{2\pi} \mathrm{d}\varphi \int \mathrm{d}\omega \sqrt{\frac{\varepsilon\left(s_0\right)v\left(s\right)}{v\left(s_0\right)Q\left(s\right)}} \exp\left[\mathrm{i}\omega\left(-\left(t-\tau\right)+\frac{1}{2}\frac{P(s)}{Q(s)}n^2\right)\right], \tag{7}$$

where φ represents the azimuth of the outgoing Gaussian beam in a point.

The reverse propagation process of the recorded seismic wavefields from the receiving point to the underground imaging point can be realized by the Kirchhoff integral (Popov et al., 2010). In other words, we construct the time-back wavefields using the upward ray tracing scheme

$$W^{(2)} = -2\int_0^{\mathrm{T}} \mathrm{d}t \int \mathrm{d}\mathbf{x}_{\mathbf{r}} P_{\mathrm{U}}(\mathbf{x}_{\mathbf{r}}, t) \frac{\partial}{\partial z} G(\mathbf{x}_{\mathbf{r}}, t - t_0; \mathbf{x}_{\mathbf{0}}) \quad , \tag{8}$$

where $G(\mathbf{x}_{\mathbf{r}}, t - t_0; \mathbf{x}_{\mathbf{0}})$ is the Green's function and $P_{\mathrm{U}}(\mathbf{x}_{\mathbf{r}}, t)$ are the observed wavefields. Under the condition of high frequency approximation, the derivative expression of it can be simplified as

$$\frac{\partial G(\mathbf{x}_{\mathbf{r}}, t - t_0; \mathbf{x}_{\mathbf{0}})}{\partial z} \approx \mathrm{i}\omega_{\mathrm{m}} p_z G(\mathbf{x}_{\mathbf{r}}, t - t_0; \mathbf{x}_{\mathbf{0}}) \quad , \tag{9}$$

where ω_{m} is the dominant frequency.

We still only consider the superposition of Gaussian beams under a single dominant frequency and use the superposition of Gaussian beams to approximate $G(\mathbf{x}_{\mathbf{r}}, t - t_0; \mathbf{x}_{\mathbf{0}})$

$$G(\mathbf{x}_{\mathbf{r}}, t - t_0; \mathbf{x}_{\mathbf{0}}) \cong -\frac{\mathrm{i}}{4\pi} \int_0^{2\pi} \mathrm{d}\varphi \sqrt{\frac{\varepsilon(s_0) v(s)}{v(s_0) Q(s)}} \exp\left[\mathrm{i}\omega_{\mathrm{m}} \left(-(t - t_0) + \frac{1}{2} \frac{P(s)}{Q(s)} n^2\right)\right]. \tag{10}$$

Substituting eq. (9) and eq. (10) into eq. (8), we can obtain the expression of time reverse wavefields

$$W^{(2)} = -\frac{\omega_{\mathrm{m}} p_z}{2\pi} \int_0^{\mathrm{T}} \mathrm{d}t \int \mathrm{d}\mathbf{x}_{\mathbf{r}} \int_0^{2\pi} \mathrm{d}\varphi P_{\mathrm{U}}(\mathbf{x}_{\mathbf{r}}, t) \sqrt{\frac{\varepsilon(s_0) v(s)}{v(s_0) Q(s)}} \exp\left[\mathrm{i}\omega_{\mathrm{m}} \left(-(t - t_0) + \frac{1}{2} \frac{P(s)}{Q(s)} n^2\right)\right]. \tag{11}$$

Parts of the expression in the time domain in the right of eq. (11) can be further simplified by Fourier forward transformation to the frequency domain

$$W^{(2)} = -\frac{\omega_{\mathrm{m}}}{2\pi} \int \mathrm{d}\mathbf{x}_{\mathbf{r}} \int_0^{2\pi} \mathrm{d}\varphi p_z P_{\mathrm{U}}(\mathbf{x}_{\mathbf{r}}, \omega) \left(\sqrt{\frac{\varepsilon(s_0) v(s)}{v(s_0) Q(s)}}\right)^* \exp\left[\mathrm{i}\omega_{\mathrm{m}} \left(t_0 + \frac{1}{2} \frac{P(s)}{Q(s)} n^2\right)\right]. \tag{12}$$

Cross-correlation imaging condition

In the migration algorithm, the imaging condition is very important, which directly affects the final imaging quality. In space-time domain, when the wavelet phases of forward and reverse wavefields are the same in the time window $t \in [t_1, t_2]$, the cross-correlation output results can reach the maximum value. And the impact of noise is reduced by the superposition of multi-shot data. In the end, we can get the space-time-domain GBM formula in VTI media based on the upward ray tracing scheme

$$I(\mathbf{x_0}) = \int \mathrm{d}\mathbf{x_s} \int_{t_1}^{t_2} \mathrm{d}t W^{(1)} W^{(2)} . \tag{13}$$

Finally, we substitute eq. (7) and eq. (12) into eq. (13), $I(\mathbf{x_0})$can be expressed as

$$I(\mathbf{x_0}) = \frac{\mathrm{i}\omega_{\mathrm{m}}}{8\pi^2} \int \mathrm{d}\mathbf{x_s} \int \mathrm{d}\mathbf{x_r} \int_0^{2\pi} \mathrm{d}\varphi \int \mathrm{d}\omega P_{\mathrm{U}}(\mathbf{x_r}, \omega) \exp\left[\mathrm{i}\omega\left(-(t-\tau) + \frac{1}{2}\frac{P(s)}{Q(s)} n^2\right)\right]$$
$$\times p_z \sqrt{\frac{\varepsilon(s_0) v(s)}{v(s_0) Q(s)}} \left(\sqrt{\frac{\varepsilon(s_0) v(s)}{v(s_0) Q(s)}}\right)^* \exp\left[\mathrm{i}\omega_{\mathrm{m}}\left(t + \frac{1}{2}\frac{P(s)}{Q(s)} n^2\right)\right] . \tag{14}$$

As shown in Fig. 2, the final migration flow chart is presented in this paper. It can be seen that the space-time-domain GBM is for each spatial point.

NUMERICAL RESULTS

In this section, we will verify the correctness of our method and its adaptability to complex models by testing anisotropic graben model, diffractor model and the field data. The shot recording data of the two velocity models are synthesized by the finite difference forward method in VTI medium, and the dominant frequency of the wavelet is 20 Hz.

Anisotropic graben model

The graben velocity model is shown in Fig. 3a, the black and red ray represent isotropic and anisotropic ray tracing, respectively. The horizontal and vertical distance are 9 km and 3 km, respectively. In this section, we only consider the second layer of the depression model as anisotropic medium, and the other layers are isotropic (Figs. 3b-c). In the forward modeling process, we use the observation system with intermediate excitation and two sides receiving and set up 301 shots with the shot spacing of 20 m. Each shot has 301 traces with the sampling of 10 m. The time

sampling interval is 0.001 s, and the total time sampling number is 2500. Fig. 4 are the imaging results in the isotropic space-time-domain GBM and the proposed method. The clear imaging results in Fig. 4b can prove the correctness of our method. When we do not consider the influence of the anisotropy, the diffraction energy of the low-end structural layer will not converge in the migration results in the blue ellipses, resulting in a decrease in the accuracy of the final migration imaging results.

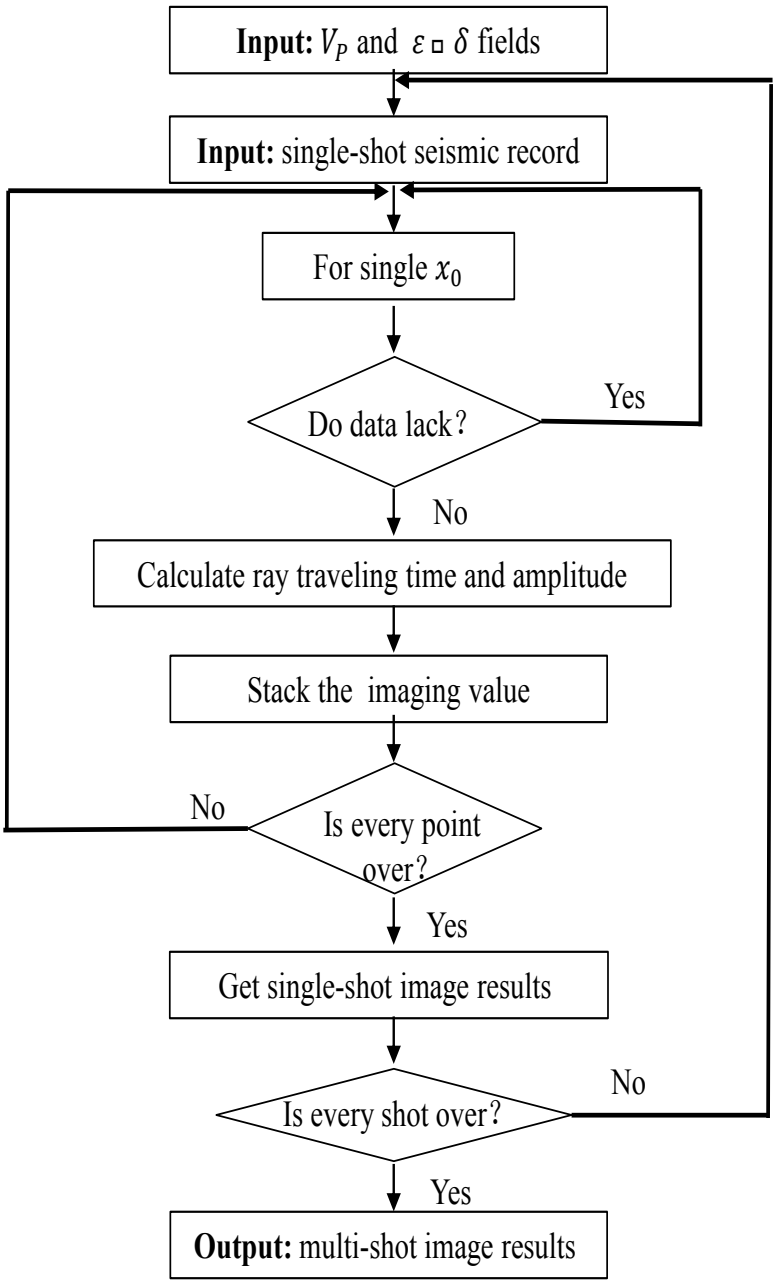

Fig. 2. The flowchart in our method.

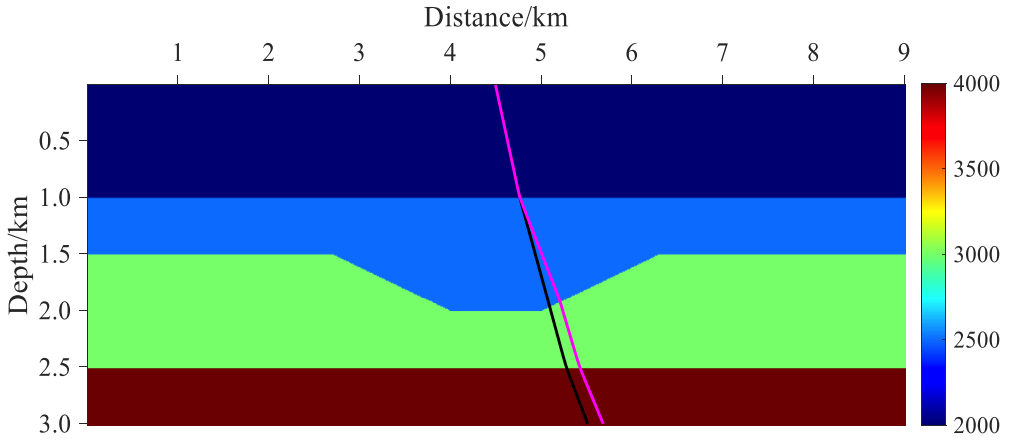

(a)

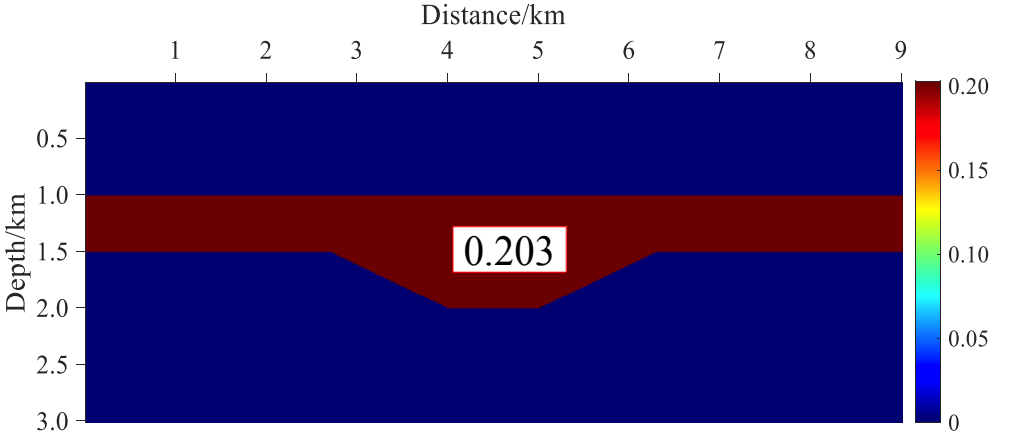

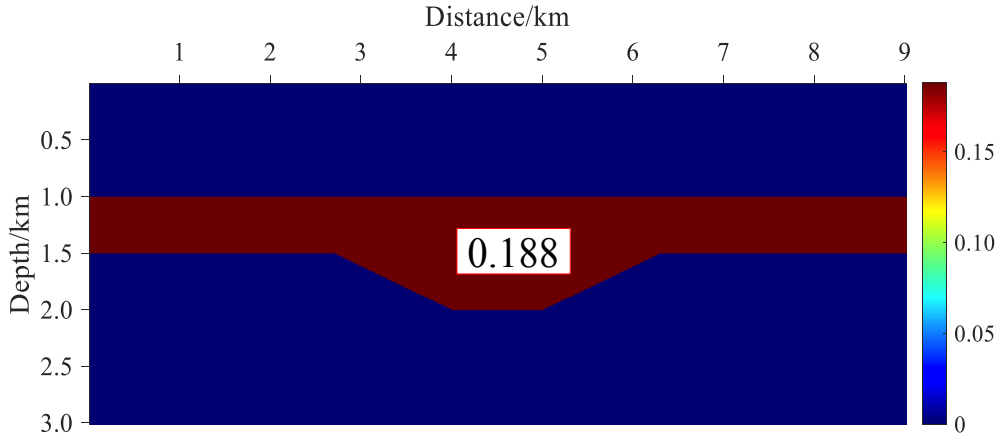

(c)

Fig. 3. Graben model. (a) v_p . (b) ε . (c) δ .

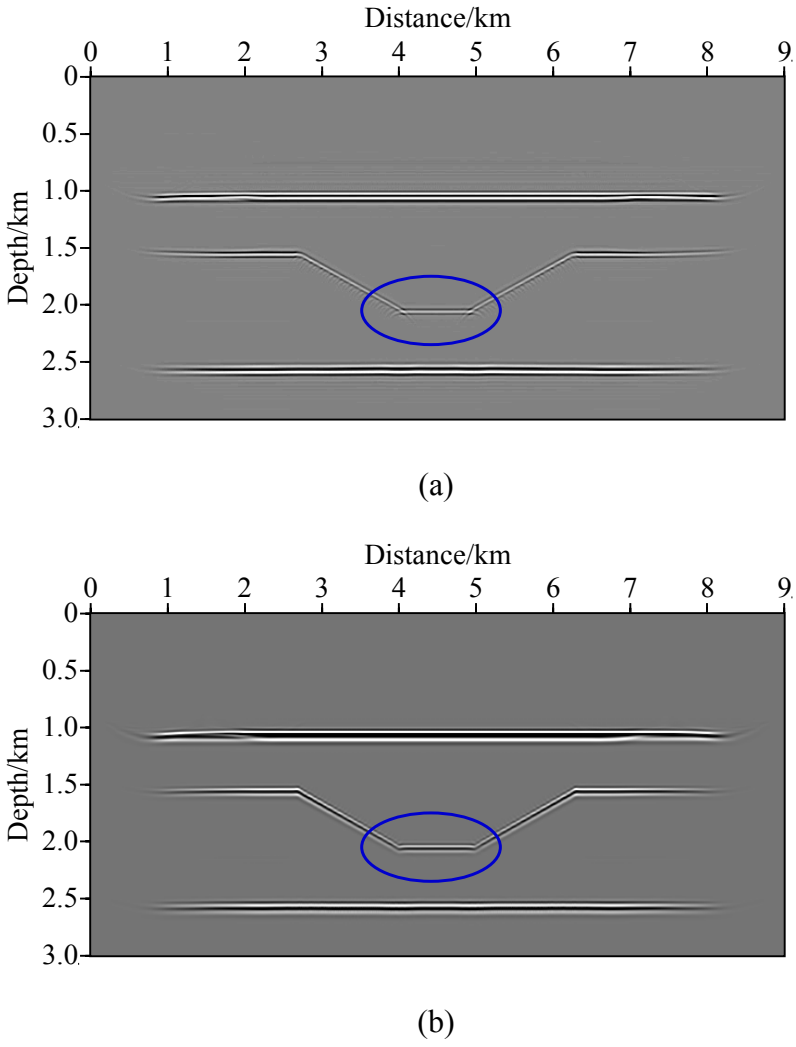

Fig. 4. Images for the graben model. (a) Space-time-domain GBM in isotropic mediea. (b) Our method.

Anisotropic diffractor model

The diffractor velocity model is shown in Fig. 5a. There are some special diffracting points based on the curved graben model. The grid size is 1201×401, and the grid spacing is 10 m. Its anisotropic parameter fields are complex as shown in Figs. 5b-5c. In the process of forward modeling, we set up 151 shots with the shot spacing of 60 m. Each shot has 301 traces, and the trace sampling is 10 m. The position of the first shot record is placed at the 151 trace. We still use the observation system with intermediate excitation and two sides receiving. The total time sampling number is 1001, and the time sampling interval is 0.003 s. Fig. 6 are the imaging results for the diffractor model in the isotropic space-time-domain GBM and the proposed method. Compared with the results in Fig. 6, our method can clearly image the special diffracting points with the results using the isotropic space-time-domain GBM (the blue ellipses). It further demonstrates the adaptability of our approach for the special model with some diffracting points.

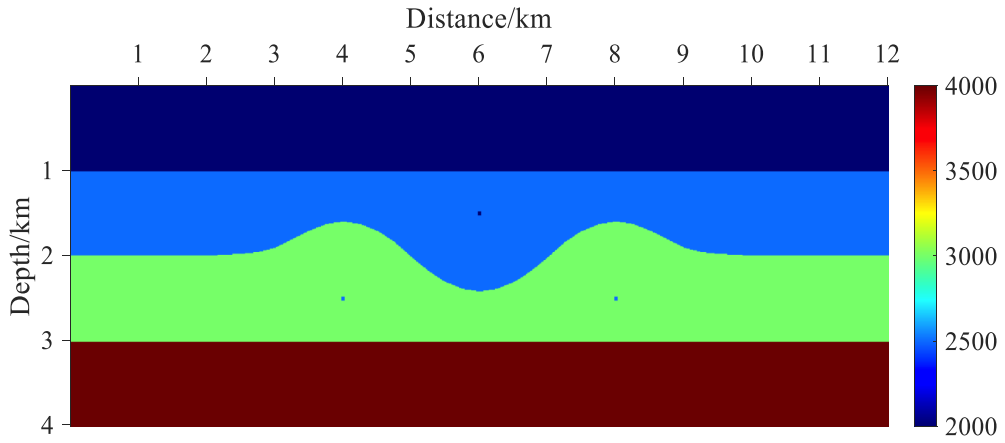

(a)

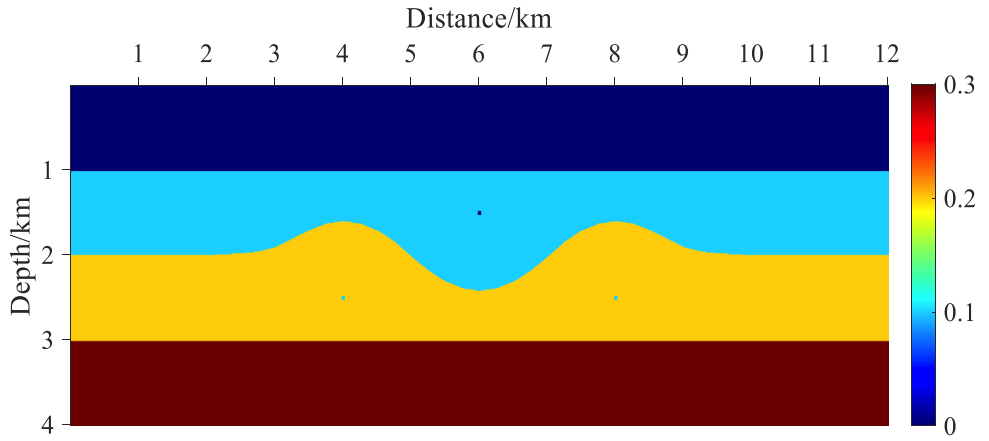

(b)

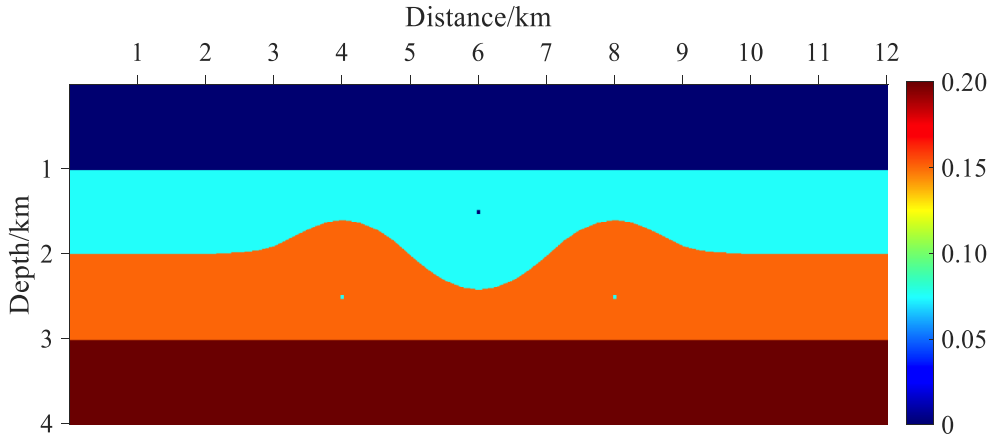

(c)

Fig. 5. Diffractor model. (a) v_p . (b) ε . (c) δ .

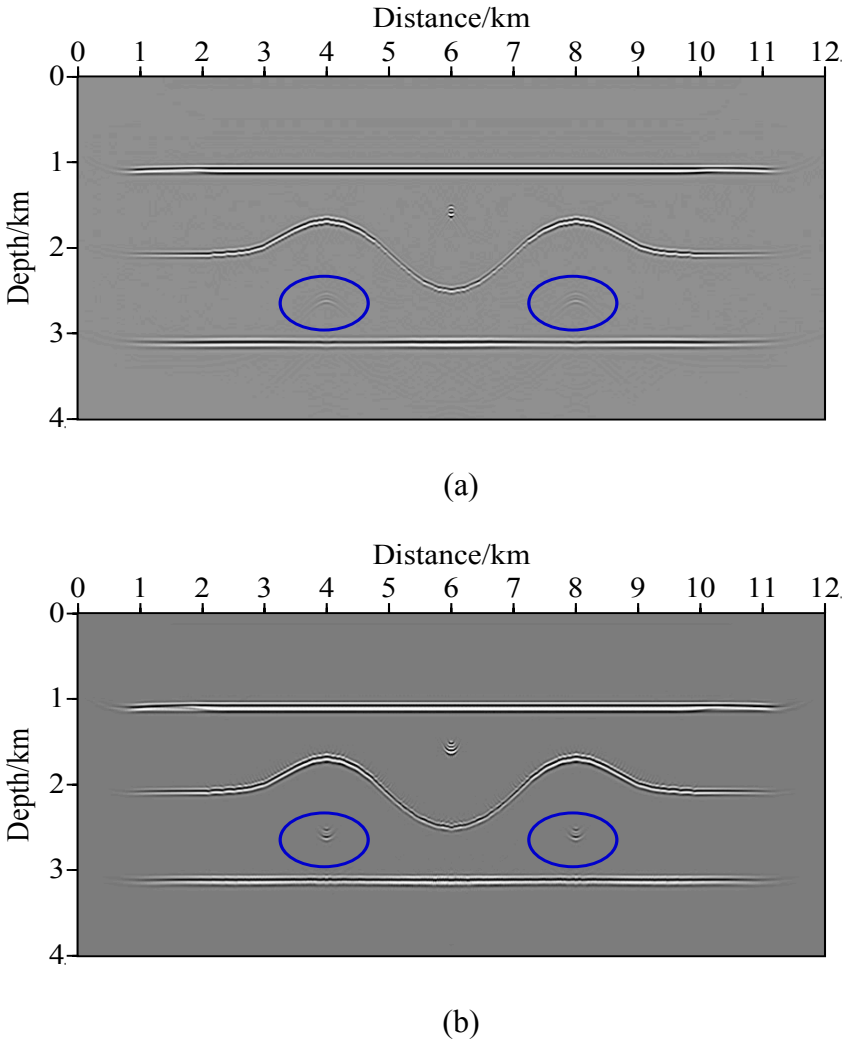

Fig. 6. Images for the diffractor model. (a) Space-time-domain GBM in isotropic media. (b) Our method.

The field data

The P-wave velocity model and anisotropic parameter fields are shown in Fig. 7. There are obvious anticline structures in the model, and the sensitivity of velocity model and anisotropic parameter fields to layers are different. The actual size of the velocity model is 25.56 km in transverse direction and 8 km in longitudinal direction. There are 264 shots, and each shot has 240 traces. The total time is 6 s, and the time sampling number is 1500. In Fig. 8, the first 1200 trace seismic record is partially missing. In the process of programming implementation, while imaging a single space point, if the corresponding seismic record is missing, the imaging value of the space point is directly given as 0, and the cycle directly jumps to the next space point. Fig. 9 are the results for the field data when we use two space-time-domain GBM methods, we see that the amplitude of the left wing of the deep anticline is more uniform (black arrows). Fig. 10 are the magnification of migration images from the red rectangle in Fig. 9, compared with the blue ellipses, the energy of the proposed method is more convergent at the top of the anticline, the resolution of the imaging results

are significantly improved, and the imaging quality is clearer. Fig. 11 are the magnification of migration images from the blue rectangle in Fig. 9, we see that the imaging results in our method have higher resolution (black arrows).

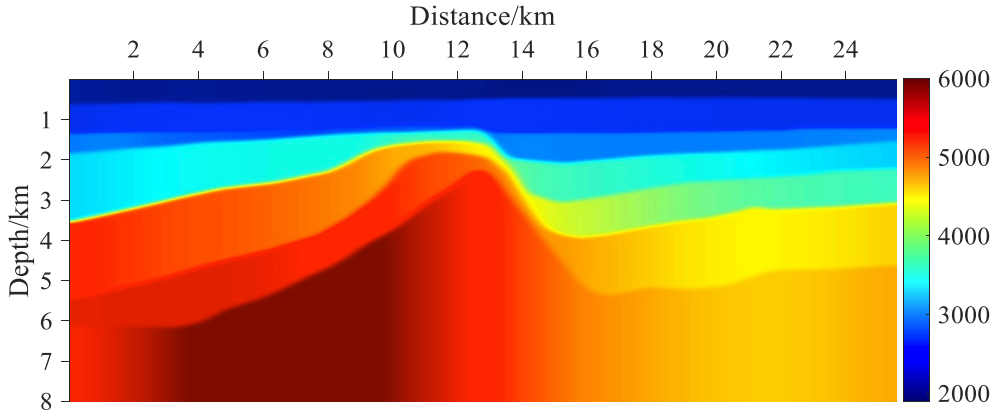

(a)

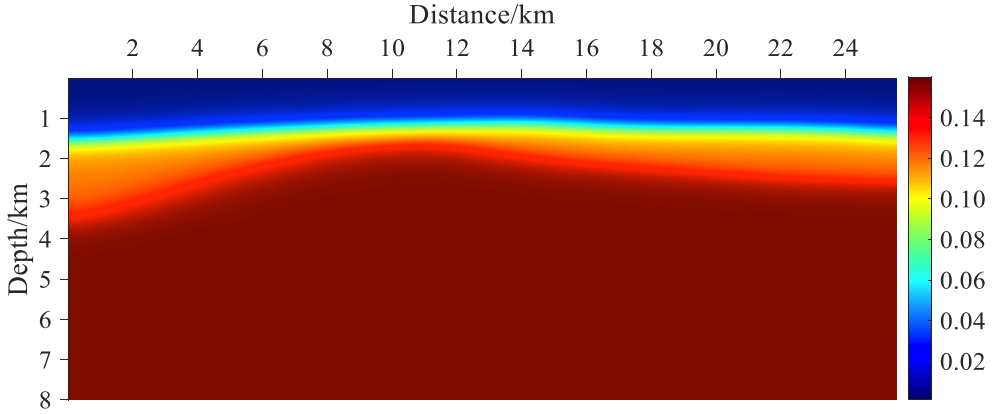

(b)

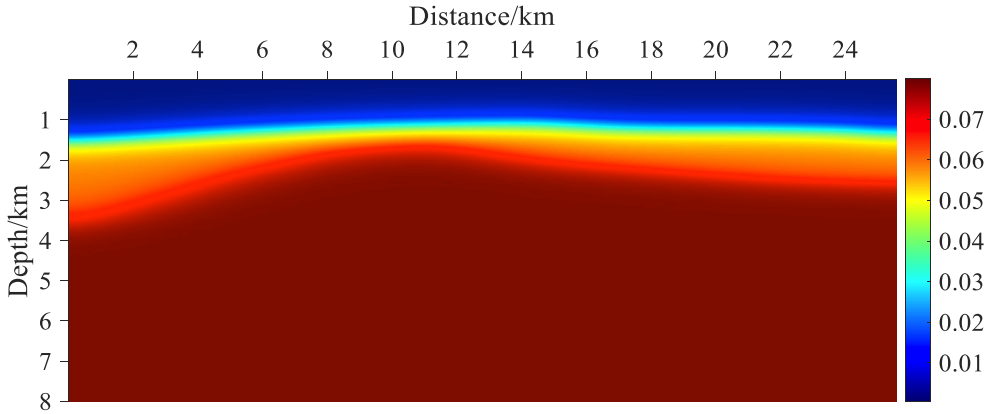

(c)

Fig. 7. The field data. (a) v_p . (b) ε . (c) δ .

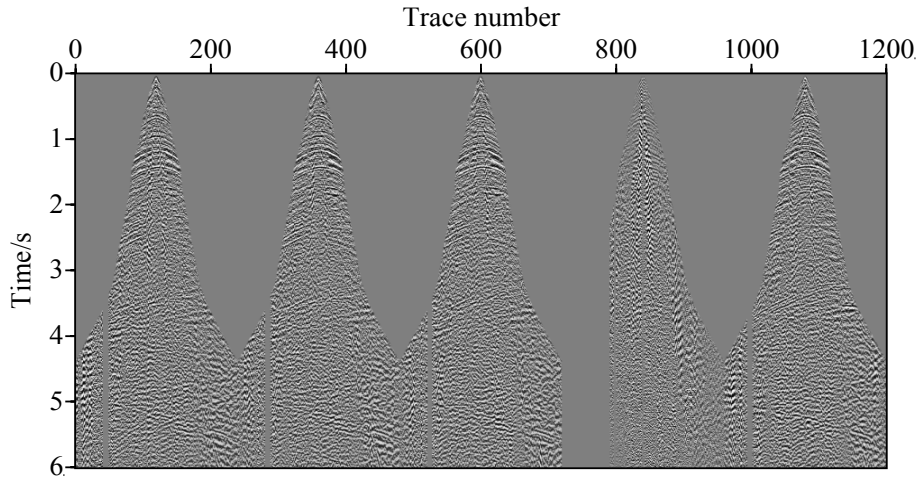

Fig. 8 The first 1200 trace seismic record for the field data.

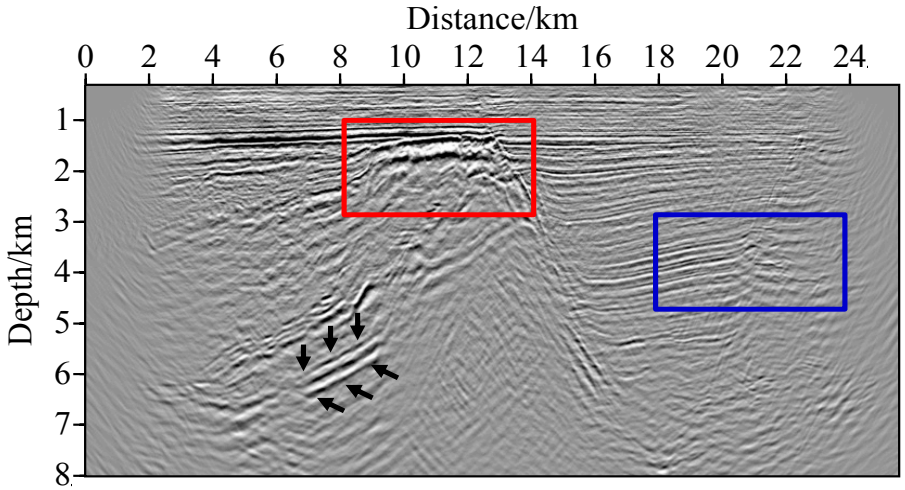

(a)

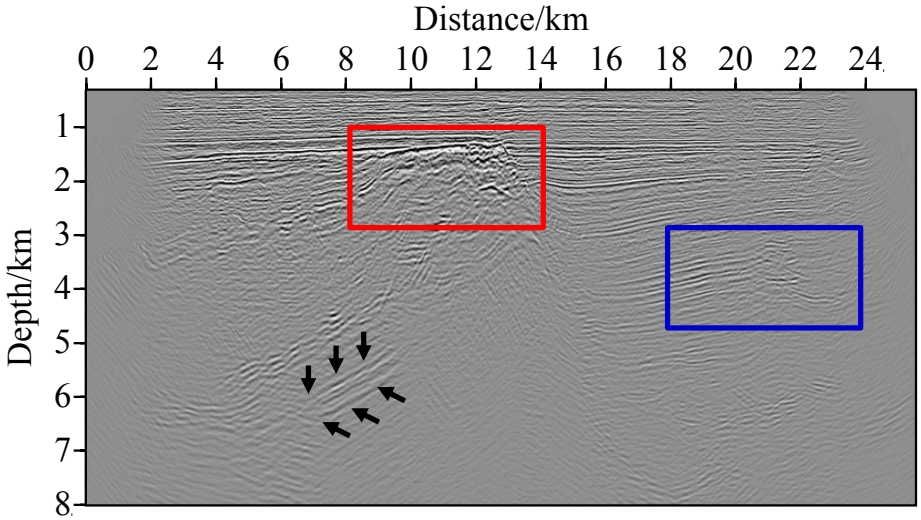

(b)

Fig. 9. Images for the field data. (a) Space-time-domain GBM in isotropic media. (b) Our method.

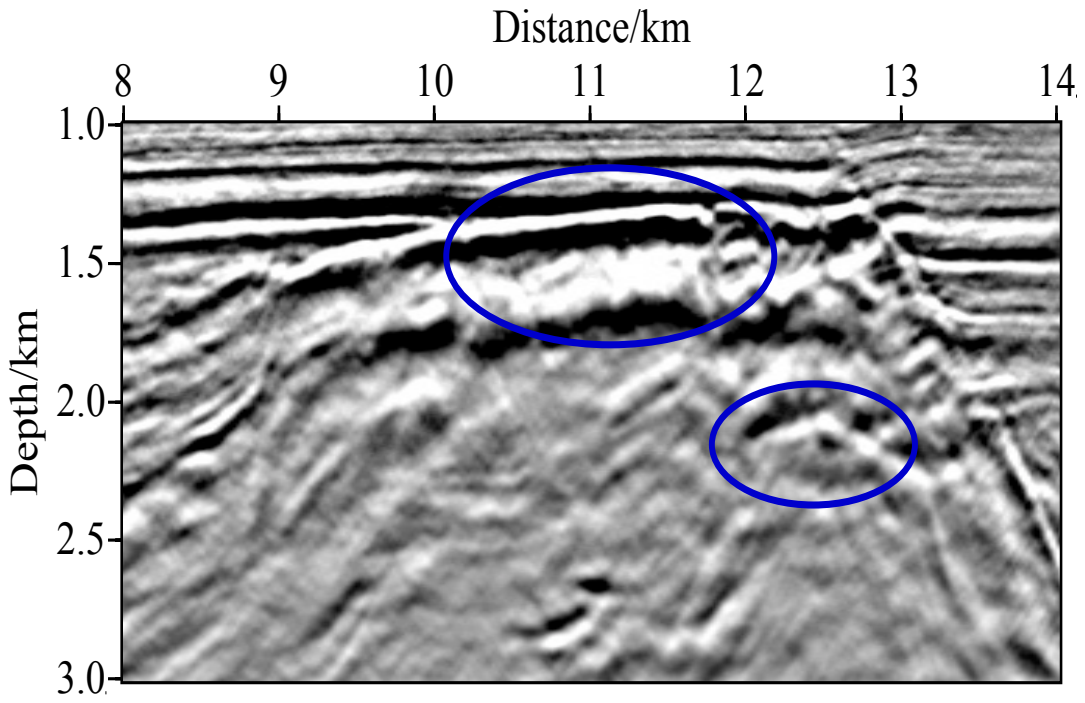

(a)

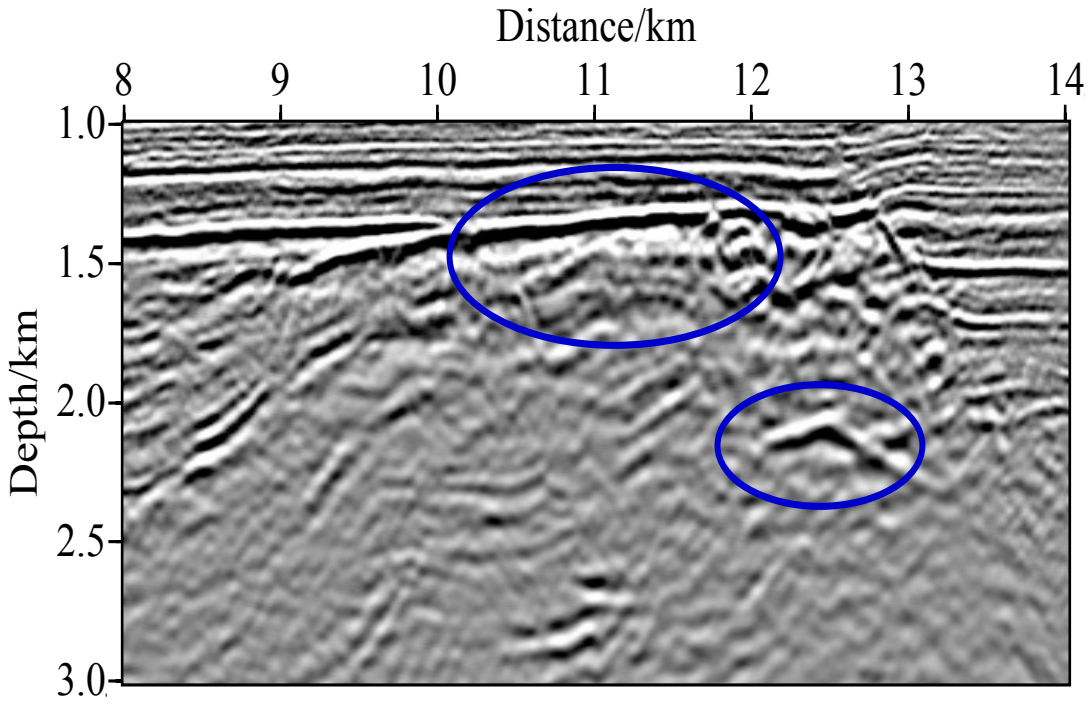

(b)

Fig. 10. Locally zoomed migration results boxed in red for the field data.
(a) Space-time-domain GBM in isotropic mediea. (b) Our method.

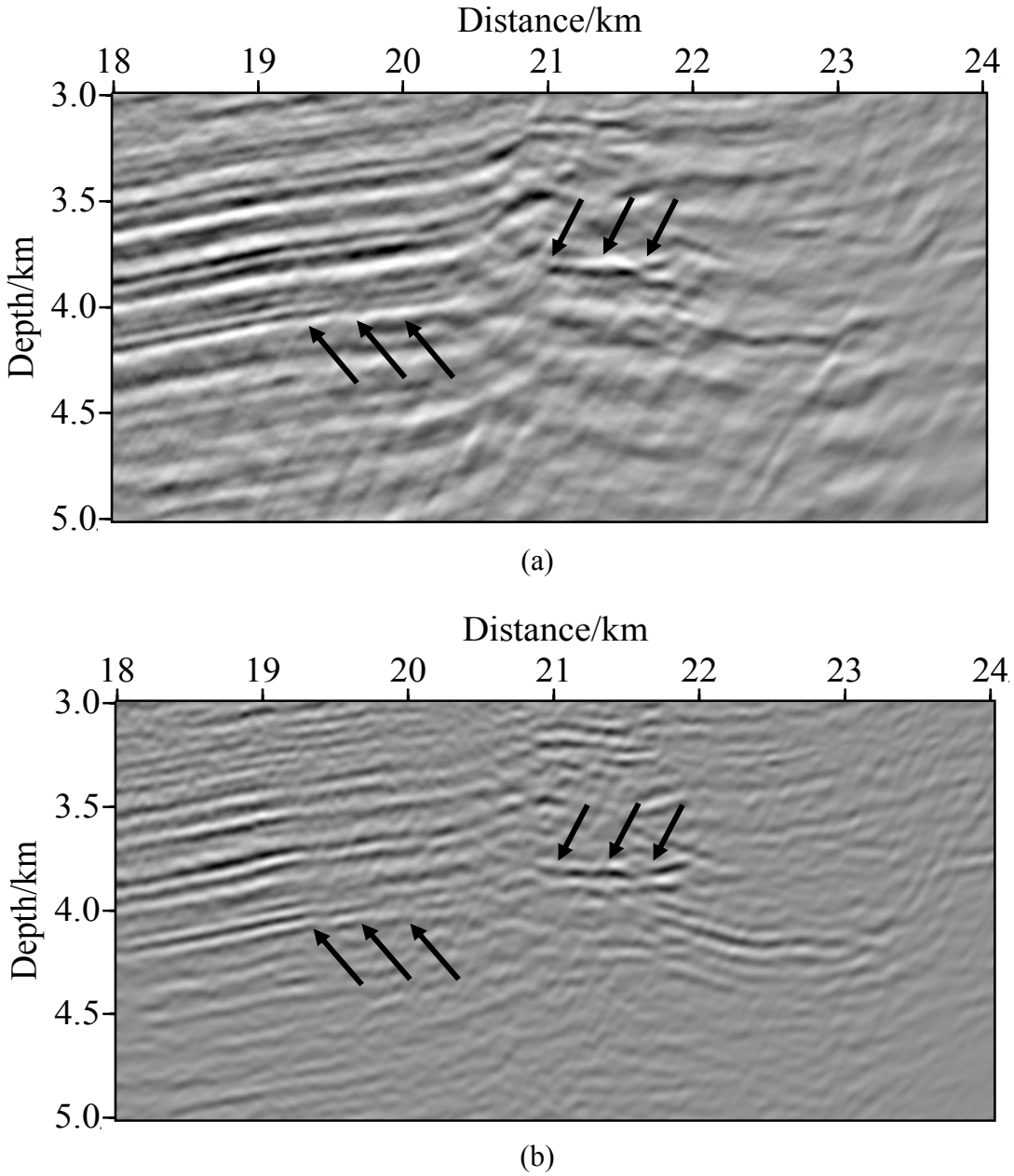

Fig. 11. Locally zoomed migration results boxed in blue for the field data.
(a) Space-time-domain GBM in isotropic mediea. (b) Our method.

CONCLUSION

In this paper, we first construct the reverse wavefields using the upward ray tracing strategy. Then the anisotropic ray tracing theory is introduced due to the complexity of underground media. Finally, we achieve a space-time-domain GBM method in VTI media based on cross-correlation imaging condition. A simple anisotropic graben model is used to verify the correctness of our method. And the adaptability of our method is further verified by the complex diffractor model and the field data. Compared with the space-time-domain isotropic GBM, the diffraction wave energy

converges in the structural layers and the in-phase axis is clearer. Our method produces more uniform amplitude of the left wing of the deep anticline and the resolution of the imaging results are significantly improved for the field data. This is the result of considering the anisotropy characteristics in this paper. Therefore, our method has better imaging accuracy and will be a good imaging tool for complex structures.

ACKNOWLEDGEMENTS

This research is supported by National Key R&D Program of China under contract number 2019YFC0605503C, The Major projects of CNPC under contract number(ZD2019-183-003), the Major projects during the 14th Five-year Plan period under contract number 2021QNLM020001, the National Outstanding Youth Science Foundation under contract number 41922028 and the Funds for Creative Research Groups of China under contract number 41821002.

REFERENCES

Alkhalifah, T., 1995. Gaussian beam depth migration for anisotropic media. Geophysics, 60: 1474-1484.

Bai, M., Chen, X., Wu, J., Liu, G., Chen, Y., Chen, H. and Li, Q., 2016. Q-compensated migration by Gaussian beam summation method. J. Geophys. Engineer., 13: 35-48.

Červený, V., 1972. Seismic rays and ray intensities in inhomogeneous anisotropic media. Geophys. J. Internat., 29: 1-13.

Červený, V., Popov, M.M. and Pšenčík, I., 1982. Computation of wave fields in inhomogeneous media-Gaussian beam approach. Geophys. J. Internat., 70: 109-128.

Gray, S.H. and Bleistein, N., 2009. True-amplitude Gaussian-beam migration. Geophysics, 74(2): S11-S23.

Han, J., Wang, Y., Xing, Z. and Lu, J., 2014. Gaussian beam prestack depth migration of converted wave in TI media. J. Appl. Geophys., 109: 7-14.

Han, J., Wang, Y., Yu, C. and Chen, P., 2017. Angle-domain common-image gathers from anisotropic Gaussian beam migration and its application to anisotropy-induced imaging errors analysis. J. Earth Syst. Sci., 126: 1-9.

Han, J., Lü, Q., Gu, B., Yan, J. and Zhang, H., 2020. 2D anisotropic multicomponent Gaussian-beam migration under complex surface conditions. Geophysics, 85(2): S89-S102.

Han, J., Liu, Z., Wang, Y., Yan, J. and Gu, B., 2021. 2D anisotropic nonslant stack beam migration for multicomponent seismic data. Arab. J. Geosci., 14(13): 1-9.

Hanyga, A., 1986. Gaussian beams in anisotropic elastic media. Geophys. J. Internat., 85: 473-504.

Hill, N.R., 1990. Gaussian beam migration. Geophysics, 55: 1416-1428.

Hill, N.R., 2001. Prestack Gaussian-beam depth migration. Geophysics, 66: 1240-1250.

Hu, Z.D., Lü, Q.D., Han, L.H., Liu, W., Huang, J.P., Yang, J.D. and Li, Z.C., 2020. Elastic space-time Gaussian beam method for seismic depth imaging. Chin. J. Geophys., 63: 652-665 (in Chinese).

Huang, J., Yang, J., Liao, W., Wang, X. and Li, Z., 2016. Common-shot Fresnel beam migration based on wave-field approximation in effective vicinity under complex topographic conditions. Geophys. Prosp., 64: 554-570.

Huang, J., Yuan, M., Zhang, Q., Jia, L., Li, Z., Li, J. and Zhao, S., 2017. Reverse time migration with elastodynamic Gaussian beams. J. Earth Sci., 28: 695-702.

Katchalov, A.P. and Popov, M.M., 1988. Gaussian beam methods and theoretical seismograms. Geophys. J. Internat., 93: 465-475.

Li, H., Wang, H.Z., Feng, B., Hu. Y. and Zhang, C., 2014. Efficient pre-stack depth migration method using characteristic Gaussian packets. Chin. J. Geophys., 57: 2258-2268 (in Chinese).

Li, Z.C., Liu, Q., Han, W.G., Zhang, M., Wang, T.Q., Xiao, J.E. and Wu, J.H., 2018. Angle domain converted wave Gaussian beam migration in VTI media. Chin. J. Geophys., 61: 1471-1481 (in Chinese).

Nowack, R.L., 2011. Dynamically focused Gaussian beams for seismic imaging. Internat. J. Geophys., 2011: 1-8.

Popov, M.M., 1982. A new method of computation of wave fields using Gaussian beams. Wave Motion, 4: 85-97.

Popov, M.M., Semtchenok, N.M., Popov, P.M. and Verdel, A.R., 2010. Depth migration by the Gaussian beam summation method. Geophysics, 75(2): S81-S93.

Protasov, M.I. and Tcheverda, V.A., 2012. True amplitude elastic Gaussian beam imaging of multicomponent walkaway vertical seismic profiling data. Geophys. Prosp., 60: 1030-1042.

Yang, J.D., Huang, J.P., Wang, X. and Li, Z.C., 2015. An amplitude-preserved adaptive focused beam seismic migration method. Petrol. Sci., 12: 417-427.

Yang, J. and Zhu, H., 2018. A practical data-driven optimization strategy for Gaussian beam migration. Geophysics, 83(1): S81-S92.

Yuan, M., Huang, J., Liao, W. and Jiang, F., 2017. Least-squares Gaussian beam migration. J. Geophys. Engineer., 14: 184-196.

Yue,, Y.B., Li, Z.C., Zhang, P., Zhou, X.F. and Qin, N., 2010. Prestack Gaussian beam depth migration under complex surface conditions. Appl. Geophys., 7: 143-148.

Yue, Y.B., Li, Z.C., Qian, Z.P., Zhang, J.L., Sun, P.Y. and Ma, G.K., 2012. Amplitude-preserved Gaussian beam migration under complex topographic conditions. Chin. J. Geophys., 55: 1376-1383 (in Chinese).

Yue, Y., Liu, Y., Li, Y. and Shi, Y., 2021. Least-squares Gaussian beam migration in viscoacoustic media. Geophysics, 86(1): S17-S28.

Žáček, K., 2006. Decomposition of the wave field into optimized Gaussian packets. Studia Geophys. Geodaet., 50: 367-380.

Zhu, T., Gray, S.H. and Wang, D., 2007. Prestack Gaussian-beam depth migration in anisotropic media. Geophysics, 72(3): S133-S138.